This is a self-archived version of an original article. This version may differ from the original in pagination and typographic details.

Author(s): Lüdeke, Sascha; Cardenas, Gabriel Duran; Hajdas, Wojtek; Jaatinen, Jukka; Kettunen, Heikki; Poivey, Christian; Rossi, Mikko; Tanios, Bendy; Vogiatzi Stergiani, Marina; Javanainen, Arto

Title: Proton Direct Ionization in Sub-Micron Technologies : Test Methodologies and Modelling

Year: 2023

Version: Published version

Please cite the original version:

Lüdeke, S., Cardenas, G. D., Hajdas, W., Jaatinen, J., Kettunen, H., Poivey, C., Rossi, M., Tanios, B., Vogiatzi Stergiani, M., & Javanainen, A. (2023). Proton Direct Ionization in Sub-Micron Technologies : Test Methodologies and Modelling. IEEE Transactions on Nuclear Science, 70(4), 667-677. https://doi.org/10.1109/tns.2023.3255008

Proton Direct Ionization in Sub-Micron Technologies:
Test Methodologies and Modelling

Sascha Lüdeke, *Student Member, IEEE*, Gabriel Durán Cardenás, Wojtek Hajdas, *Member, IEEE*, Jukka Jaatinen, Heikki Kettunen, *Member, IEEE*, Christian Poivey, *Member, IEEE*, Mikko Rossi, Bendy Tanios, Stergiani Marina Vogiatzi *Member, IEEE,* and Arto Javanainen, *Member, IEEE*

Abstract—Two different low energy proton (LEP) test methods, one with quasi-monoenergetic and the other with very wide proton beam energy spectra, have been studied. The two test methodologies have been applied to devices that were suggested from prior heavy-ion tests to be sensitive to proton direct ionization (PDI). The advantages and disadvantages of the two test methods are discussed. The test method using quasi-monoenergetic beams requires device preparation and high energy resolution beams, but delivers results that can be interpreted directly and can be used in various soft error rate (SER) calculation methods. The other method, using a heavily degraded high energy proton beam, requires little to no device preparation but more efforts on the beam characterization, and is confined to a specific SER method. While both methods deliver comparable estimates on the SER, the relatively complex determination of the beam characteristics in the degraded beam method makes it less straightforward to use. This work furthers presents a method to extract PDI sensitive volume parameters from degraded high energy proton beam cross-section data. This method extends the use of a previously published method to the degraded high energy beam LEP testing method.

Index Terms—proton direct ionization (PDI), single event upset (SEU), heavy ions (HI), soft error rate (SER), degraded high energy protons (DHEP), numerical fitting, rectangular parallelepiped (RPP)

I. INTRODUCTION

THE impact of heavy ions (HI) and high energy protons (HEP) on the performance of electrical devices under irradiation has been studied in the past [1]–[7]. However, the impact of proton direct ionization (PDI) SEUs caused by low energy protons (LEP) on modern highly scaled sub-micron technologies has become an increasingly important

issue [8]–[28]. Since not all devices, even those with smaller technology node sizes, exhibit sensitivity to PDI [29]–[34], the necessity of LEP testing for a given device is not easily assessed. A common assumption whether a device could possibly be sensitive to PDI SEUs is based on the linear energy transfer (LET) threshold value LET_0 obtained from the Weibull-fit of HI test data. Typically, when the threshold LET is below the peak LET of protons ($\sim 0.5\,\mathrm{MeVcm^2/mg}$), PDI sensitivity is considered likely. However, the most reliable way to determine PDI sensitivity is to perform LEP testing.

The common approach to test the LEP SEU response of a device is to expose it to LEP beams with well-defined energies [8]–[26], [29]. In this work, these beams are referred to as quasi-monoenergetic (QME). These tests are performed very similar to the conventional HI and HEP tests, and require access to an accelerator that can provide these low energy beams with high energy resolution. Also preparation of the devices under test is required to enable the low energy protons to reach the sensitive volume within the device. Soft error rates (SER) can be calculated from the results of QME tests via a variety of methods. In this work the following three SER approaches are used: Energy Multiplication Method (EMM), Energy Integration Method (EIM), and Sensitive Volume Method (SVM) (see IV).

Another LEP test method, alternative to the QME approach, using strongly degraded proton beams, was proposed by Dodds *et al.* in [28], and further discussed in [27]. However, the first consideration of using this kind of test method was as early as 2012 [35]. For this method, in this work referred to as degraded high energy proton (DHEP), a high-energy proton beam (i.e., tens of MeV) is strongly degraded using thick degraders to produce a wide proton energy spectrum. The obtained spectrum should be well known, by measurement and/or simulations, and contain energies in the LEP energy range of less than $3\,\mathrm{MeV}$. As discussed in the original work by Dodds *et al.*, the main purpose of this method is to provide estimates for PDI SERs for radiation environments behind shielding without the necessity of using the QME test method and the associated need for a LEP beam facility. This SER method will be referred to as the DHEP Method in this work (see IV). Therefore, this method only applies when the degraded proton beam spectrum and

the investigated radiation environment spectrum have similar shapes for energies below 3 MeV, because protons below 3 MeV are considered to predominantly contribute to the LEP SER according to this test methodology [28].

Being presented with two different methods to perform LEP testing and to calculate LEP SERs based on the results, it is important to understand the advantages and disadvantages of both methods as well as the amount of preparation and effort during data evaluation associated with either. Important questions are: Does the DHEP method provide a suitable alternative for SER calculations when access to a LEP facility is limited or unavailable, and is it possible to gain also other information from that method than the SER for degraded radiation environments?

To answer these questions, irradiation tests have been performed for the SRAM components of two devices from different manufacturers. The tests include HI, QME LEP, HEP and DHEP tests. The goals of this study are to:

1.) Compare the testing procedures of QME and DHEP testing in terms of preparation, data processing and SER calculation.
2.) Investigate a method to extract PDI sensitive volume (SV) parameters from the DHEP test data.

The second goal of this study is based on the method to extract PDI SV parameters from QME data presented in [36]. In this work, the method is shown to extract PDI SV parameters from DHEP data as well. As in the previous work [36], the method extracts parameters for a single SV, or also referred to as the PDI SV or PDI RPP geometry in this work.

II. EXPERIMENTAL INVESTIGATION

A. Devices Under Test

The devices under test (DUT) in this work are the SRAM memories of two devices from different manufacturers, referred to in this work as ISSI and Lattice. The technology sizes are 40 nm and 28 nm, respectively. A more detailed description of the DUTs is given in Table I. All devices were delidded prior to testing and operated at nominal voltage. Previous LEP irradiation results for the ISSI device were published in [9] and [14].

B. Heavy Ion Tests

The heavy-ion tests were performed at the *RADiation Effects Facility* (RADEF) [37] in Jyväskylä, Finland, for both devices. For this work, the following ions from the 16.3 MeV/u ion cocktail were used: O, Ne, Ar, Fe, Kr and Xe. Additional 8.9 MeV/u Li data was taken at UCL, Belgium [38], with an LET of 0.35 MeVcm²/mg. Irradiations were performed in vacuum under normal incidence as well as under tilt to cover a wider effective LET range. The heavy ion tests were conducted to fully characterize the devices used in this work. The determined threshold LET from the results of the HI tests are used later in this work to support the extraction of the PDI SV parameters from the DHEP data.

C. Low Energy Proton Tests

The LEP tests were performed at RADEF [39] for both devices. All devices were tested at normal incidence. The energies, fluences and resulting doses of the irradiation test are given in Table II. Irradiations were performed in vacuum.

D. High Energy Proton and Degraded Beam Tests

The HEP and DHEP tests were performed at the *Paul-Scherrer Institut* (PSI), Villingen, Switzerland. Specifically at the Proton Irradiation Facility (PIF) [40]. The energy of the primary proton beam was 71.1 MeV for the HEP and DHEP tests. The beam was degraded using a combination of Cu and Al slabs, with thicknesses up to 7.0 mm and 1.5 mm, respectively. The tests were performed in air.

For the HEP tests, the initial proton beam was used nondegraded as well as degraded by using Cu degraders. For these Cu degrader configurations the energy spectra of the resulting beam is well known by the facility and qualifies for reliable HEP testing. Additional Al degraders were introduced into the beam line together with the already present 7 mm of Cu to create the heavily degraded proton beams used for the DHEP method. For this strong degradation, additional beam flux and spectra measurements were necessary, because these configurations are not commonly used at the facility. The beam spectrum and flux at device level were measured using a NaI detector. The flux was measured for all degrader configurations, but due to time constraints the energy spectrum was only measured for four degrader configurations (IV-VII, see Table III).

Table III shows the degrader configurations and corresponding mean beam energies and FWHM used for the HEP and DHEP tests. The average energies for the HEP and DHEP beams were derived from Geant4 simulations (see Section III-C).

III. IRRADIATION RESULTS

In the following section the results of the irradiations performed in this work are presented. The data shown in the following figures include vertical error bars representing the 95 % confidence interval. When the error bars are not visible in the graphs, they are smaller than the size of the marker.

A. Heavy Ions

The measured SEU cross-sections for HI for both DUTs are displayed in Fig. 1. The cross-section in cm²/bit is given as a function of effective LET (LET_{eff}) in MeVcm²/mg. The effective LET is calculated after

$$LET_{eff} = \frac{LET}{cos(\theta)}, \qquad (1)$$

where LET is the linear energy transfer of the ion under normal incidence and θ the tilt angle. Furthermore, a Weibull fit was applied to the data sets. The Weibull parameters and the results of the χ^2-tests of the fits are given in Table IV.

TABLE I
SPECIFICATIONS OF THE DUTs.

Name	Part Description	Device Type	Node Size	Memory Size	Overlayers
ISSI	*ISSI IS61WV204816BLL-10TLI*	CMOS SRAM	40 nm	3.3×10^7 Bits	∼6 µm
Lattice	*Lattice LIFCL-17-7SG72C*	CMOS SOI SRAM (FPGA)	28 nm	3.1×10^6 Bits	∼9 µm

B. Quasi Mono-Energetic Protons

Figures 2 and 3 present the experimental SEU cross-section data from the QME LEP and HEP tests for both DUTs studied in this work. The SEU cross-section σ in $\mathrm{cm}^2/\mathrm{bit}$ is given as a function of the proton energy E at device level in MeV. Additionally, graphical representations of the approximations of the PDI cross-section response used for the LEP SER calculation methods given in IV are presented in Figs. 2 and 3: EMM, EIM, SVM, and DHEP Method.

The SEU response of the ISSI device (Fig. 2) shows a four orders of magnitude difference in cross-section between the

TABLE II
LEP IRRADIATION TEST PARAMETERS

Device	Energies [MeV]	Fluence [cm^{-2}]	Dose [krad]
ISSI	$0.55 - 3.3$	$(5.56 \pm 4.49) \cdot 10^7$	0.163 ± 0.103
	3.3	$3.59 \cdot 10^9$	4.01
Lattice	$0.8 - 5.5$	$(0.58 \pm 1.71) \cdot 10^{10}$	8.01 ± 12.83

TABLE III
AVERAGE PROTON BEAM ENERGY USED AT THE PROTON TESTING AT PSI FOR THE DIFFERENT DEGRADER CONFIGURATIONS. THE TESTED DEVICES FOR EACH DEGRADER CONFIGURATION ARE GIVEN.

	d_{Cu} [mm]	d_{Al} [mm]	E_{mean} [MeV]	$FWHM$ [MeV]	Devices tested
HEP					
I	-	-	70.7	2.61	ISSI, Lattice
II	3.0	-	53.3	2.50	ISSI, Lattice
III	6.5	-	21.7	4.55	ISSI, Lattice
DHEP					
IV	7.0	-	9.84	12.76	ISSI, Lattice
V	7.0	0.2	8.00	15.21	ISSI
VI	7.0	0.4	6.30	15.21	ISSI
VII	7.0	0.6	4.99	13.00	ISSI, Lattice
VIII	7.0	1.0	3.41	8.22	ISSI, Lattice
IX	7.0	1.5	2.48	5.09	ISSI, Lattice

TABLE IV
WEIBULL FIT PARAMETERS

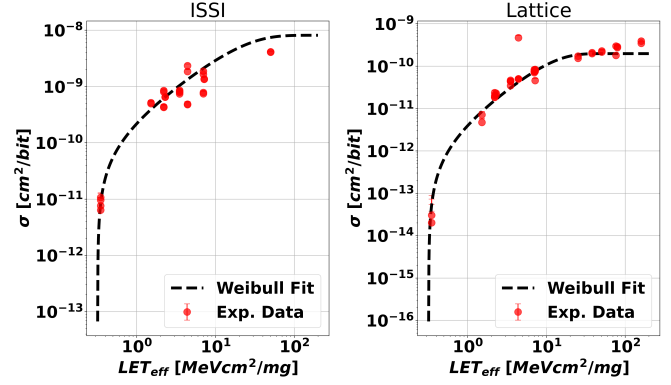| Device	σ_{sat} [cm^2/bit]	LET_0 [MeVcm^2/mg]	W [-]	S [-]	χ^2 [cm^2/bit]
ISSI	$8.11 \cdot 10^{-9}$	0.32	21.14	1.05	0.17
Lattice	$1.97 \cdot 10^{-10}$	0.32	11.58	1.38	1.26

Fig. 1. Measured HI SEU cross-sections for the two devices tested in this work as a function of effective LET. A Weibull function was fitted to the experimental data and is displayed in the graphs.
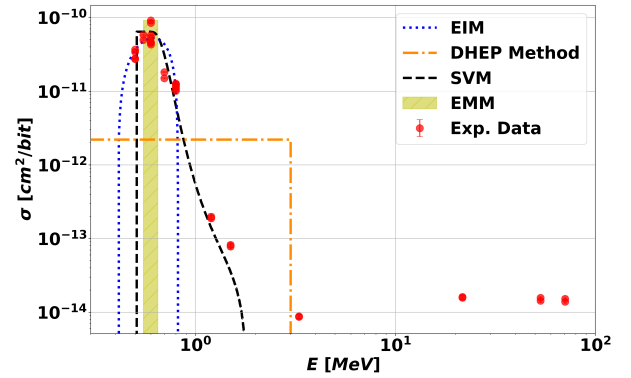

Fig. 2. The measured proton SEU cross-section σ data for the ISSI memory in $\mathrm{cm}^2/\mathrm{bit}$ is presented over the incoming proton energy E in MeV at device level (red circles). Graphical representations of the SER methods investigated in this work are displayed (see IV).

LEP and HEP regimes and is therefore considered to be very sensitive to PDI.

The Lattice memory (Fig. 3) does exhibit elevated SEU cross-section values in the LEP regime, but not as prominently as the ISSI device. The cross-section values for the Lattice DUT are approximately two orders of magnitude higher at low proton energies compared to those at high energies. Therefore, the device is considered to be moderately sensitive to PDI.

C. Degraded High Energy Proton

The results of the degraded proton beam irradiation campaign are presented in Fig. 4. The SEU cross-section σ is given in $\mathrm{cm}^2/\mathrm{bit}$ as a function of the mean beam energy E_{mean} in MeV or the corresponding degrader configuration (see Table III).
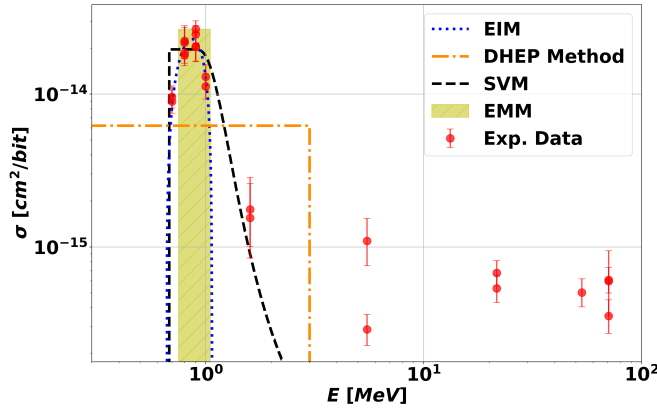
Fig. 3. The measured proton SEU cross-section σ data for the Lattice memory in $\mathrm{cm}^2/\mathrm{bit}$ is presented over the incoming proton energy E in MeV at device level (red circles). Graphical representations of the SER methods investigated in this work are displayed (see IV).
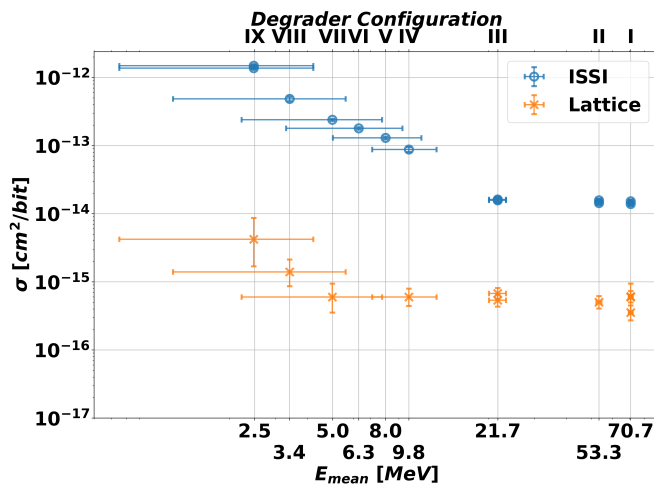

Fig. 4. Measured DHEP and HEP SEU cross-sections σ in $\mathrm{cm}^2/\mathrm{bit}$ as a function of mean beam energy E_{mean} in MeV or the degrader configuration given in Table III. The horizontal error bars represent the FWHM of the energy spectra associated with the degrader configurations.

Both the ISSI and the Lattice device exhibit increasing cross-section with increasing degrader thickness, i.e., decreasing mean energy. For both devices the maximum cross-section occurs at degrader configuration IX (7 mm Cu and 1.5 mm Al). The increase in cross-section is more pronounced for ISSI compared to Lattice.

During the DHEP tests, the energy spectra of the degraded beams were measured for configurations IV-VII (see Table III). The detector was calibrated using a Co60 source and measured background spectra were subtracted. Due to the subtraction of the background radiation and the limits of the detector and the data acquisition setup, the measured spectra lack reliable data below $\sim 2\,\mathrm{MeV}$. To resolve the lack of data, that are needed for the SER calculations and the reconstruction of the quasi mono-energetic LEP response later in this work, simulations of the beam line and degrader configurations were performed to reproduce the measured degraded spectra. The materials and their thicknesses used

in the degrader setup can be seen in Table V. The primary energy of the proton beam was set to $71.1\,\mathrm{MeV}$ in the simulations. The simulations were performed with the G4SEE toolkit [41], that is based on Geant4 [42].

TABLE V
DESCRIPTION OF THE DEGRADER MATERIALS AND THICKNESSES USED
IN WORK TO SIMULATE THE DHEP BEAMS AT PSI.

	DUT
Air	18.0 cm
Al	variable (0.0/0.2/0.4/0.6/1.0/1.5 mm)
Air	3.0 cm
Cu	7.0 mm
Air	17.0 cm
	Beam exit

The simulated and the measured spectra are presented in Fig. 5. The agreement of the spectra is overall acceptable and improves with increasing Al-degrader thickness. Due to the limitations of the simulations software, the Cu collimator, present at the beam line in the experiments, could not be simulated. Therefore, the simulated spectra do not take into account the low energy protons scattered from the collimator. This scattering effect is assumed to be the reasons behind the mismatch between simulated and measured spectra at low energies. This effect is more pronounced for configurations with less degrader material for which the particle counts at low energies are lower compared to the more degraded spectra. Furthermore, the smaller the degrader thickness the higher the relative thickness uncertainty, which could have an impact on the agreement of the measured and simulated spectra at the lower degrader thicknesses. Overall, the simulation set-up reproduces the measured spectra accurately enough for higher degrader thicknesses and is therefore trusted to estimate the spectra for configurations VIII and IX, for which no measured data are available. The simulated spectra are used in the SER calculations and the extraction of the devices' PDI SV parameters from the DHEP data.

IV. SOFT ERROR RATE CALCULATIONS

In the following sections, four SER calculation methods for the two LEP testing methods are presented, three for the QME method and one for the DHEP method. Then, SERs for the two devices exhibiting PDI sensitivity are calculated for two radiation environments using the methods described here. The different approaches are compared against each other and discussed.

A. Methods

The first three methods, *EMM*, *EIM* and *SVM*, use the QME cross-section data and the last method, *DHEP Method*, the DHEP cross-section data. In the following, $\Phi_{env}(E)$ represents the isotropic differential proton energy flux in $(\mathrm{MeV\,cm}^2\mathrm{s})^{-1}$ for the radiation environment under investigation. For this work, two radiation models were used to calculate the SERs. A geosynchronous equatorial orbit
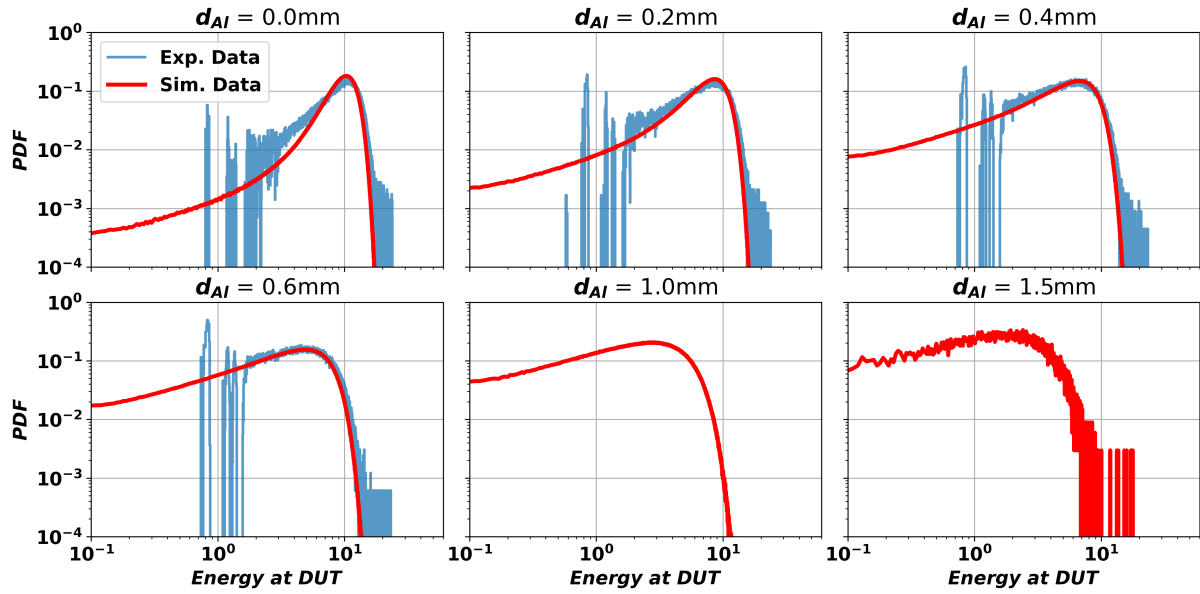
Fig. 5. Measured (blue) and simulated (red) degraded beam spectra of the $\sim71.1\,\mathrm{MeV}$ energy proton beam at PSI. The probability density function (PDF) of the spectrum is given over the energy at DUT position. The general degrader configuration is given in Table V and the added Al degrader is given in the graph.

(GEO) under solar maximum conditions and a low earth orbit (LEO) under solar minimum conditions. Both were calculated behind three different shielding thicknesses using CREME96. These radiation environments were chosen to have spectra of similar shape to the degraded proton beam spectra below $3\,\mathrm{MeV}$ as required by the DHEP SER method [28].

1) Energy Multiplication Method (EMM): In this method the maximum PDI cross-section σ_{peak} at energy E_{peak} and the full width at half maximum $FWHM$ of the PDI cross section peak are estimated from the QME LEP test results [29]. The SER τ_{EMM} is then calculated using

$$\tau_{EMM} = \sigma_{peak} \cdot \Phi_{env}(E_{peak}) \cdot FWHM. \qquad (2)$$

The $FWHM$, E_{peak} and σ_{peak} estimated for the two devices studied in this work can be found in Table VI. A graphical representation of this fit to the PDI peak based on the parameters of this method can be seen in Figs. 2 and 3, where it is referred to as *EMM*.

For this method, FWHM was derived visually from a linear-linear plot of the experimental cross-section data. This was done deliberately in such a manner to distinguish this approach from the next. This approach is meant to be a *Pen-And-Paper* approach, that needs no external software or coding to derive the SER.

2) Energy Integration Method (EIM): For this method, a second order polynomial fit σ_{2nd} is applied to the quasi mono-energetic PDI cross-section peak [34]:

$$\sigma_{2nd}(E) = A \cdot (E_{max} - E) \cdot (E - E_{min}) \qquad (3)$$

The zeros of σ_{2nd} are designated E_{min} and E_{max} and A is a fitting factor in $\mathrm{cm}^2/\mathrm{MeV}^2$. The SER τ_{EIM} is calculated as follows

$$\tau_{EIM} = \int_{E_{min}}^{E_{max}} \sigma_{2nd}(E) \cdot \Phi_{env}(E)dE. \qquad (4)$$

The parameters for σ_{2nd} and the results of the χ^2-test of the fit for the two DUTs can be found in Table VI. The graphical representation of the fit to the PDI peak proposed by this method can be seen in Figs. 2 and 3, where it is referenced as *EIM*.

3) SV Method (SVM): For this SER method, the method presented in [36] is used to estimate the PDI response curve based on PDI rectangular parallelepiped (RPP) sensitive volume (SV) parameters for both DUTs. The resulting function is referred to here as $\sigma_{PDI,method}(E)$. This estimated response can then be used similarly to the Weibull-fit to calculate the SER:

$$\tau_{SVM} = \int_{0}^{\infty} \sigma_{PDI,method}(E) \cdot \Phi_{env}(E)dE \qquad (5)$$

The determined PDI SV parameters for the two devices can be seen in Table IX. A graphical representation of the fit to the PDI peak by this method can be seen in Figs. 2 and 3, where it is referenced as *SVM*.

4) Degraded High Energy Proton Beam Method (DHEP): For the degraded proton beam data [28] proposed the following SER method to calculate the LEP SER. For this method, the degrader configuration for which the DUT exhibits the maximum cross-section σ_{max} (not to be confused with the peak of the PDI response σ_{peak}) is to be identified and the experimental flux at the DUT level Φ_{exp} for that degrader configuration determined, either via measurement or simulation.

This SER method aims to calculate the error rate caused by protons reaching the DUT at energies below $3\,\mathrm{MeV}$ [28].

Therefore, the measured σ_{max} has to be adjusted to account for the contribution in cross-section by the high energy protons reaching the device. The saturated high energy proton cross-section is orders of magnitude lower than the PDI cross-section peak (see Figs. 2 and 3). The high energy protons in the beam spectra contribute to the flux but not as much to the number of upsets in the device compared to the LEPs, thereby reducing the resulting cross-section for that degrader configuration. To account for this effect, σ_{max} is adjusted by the ratio of sub $3\,\mathrm{MeV}$ protons to protons of all energies [28]:

$$\sigma_{adj} = \sigma_{max} \cdot \left(\frac{\int_0^\infty \Phi_{exp}(E)\ dE}{\int_0^{3\,\mathrm{MeV}} \Phi_{exp}(E)\ dE} \right) \quad (6)$$

The adjusted cross-section σ_{adj} is used to calculate the SER τ_{DHEP} with the radiation environment under investigation Φ_{env}:

$$\tau_{DHEP} = \sigma_{adj} \cdot \int_0^{3\ MeV} \Phi_{env}(E)dE \quad (7)$$

The adjusted cross-sections determined for the two DUTs can be found in Table VI. A graphical representation for the assumed LEP response by this approach is given in Fig. 2 and 3, where it is referenced as *DHEP Method*.

TABLE VI
SER CALCULATION METHODS PARAMETERS.

Device	ISSI	Lattice
FWHM [MeV]	0.1	0.3
E_{peak} [MeV]	0.6	0.9
σ_{peak}[cm^2/bit]	$9.12 \cdot 10^{-11}$	$2.66 \cdot 10^{-14}$
A [cm^2/MeV^2/bit]	$1.25 \cdot 10^{-9}$	$5.44 \cdot 10^{-13}$
Emin [MeV]	0.41	0.66
Emax [MeV]	0.82	1.07
χ^2[cm^2/bit]	$4.5 \cdot 10^{-21}$	$5.1 \cdot 10^{-29}$
σ_{adj} [cm^2/bit]	$2.20 \cdot 10^{-12}$	$6.21 \cdot 10^{-15}$

B. Results & Discussion

The results of the SER calculations for the ISSI and Lattice devices are presented in Tables VII and VIII, respectively. In addition to the quantitative SER results, the ratio of the different SER methods to τ_{SVM} are given.

Overall, the results of the different SER calculation methods show decent agreement with each other in terms of SER. For the ISSI device, the different QME SER methods provide very similar results. except for τ_{EMM}. The DHEP method results in SER that are on average $\sim25\,\%$ lower than the QME SVM and EIM results. For the Lattice device, the results of the three QME SER methods vary more than for the other device. The lowest SER, τ_{EIM}, and the highest SER, τ_{DHEP}, differ by a factor of four. With increasing PDI sensitivity of the device, the different SER methods appear to agree more in their predictions.

TABLE VII
SER FOR THE ISSI DUT FOR THE LEO AND GEO RADIATION ENVIRONMENTS BEHIND VARIOUS SHIELDING THICKNESSES AFTER THE FOUR METHODS PRESENTED. ALSO THE AVERAGE RATIO OF THE DIFFERENT METHODS TO τ_{SVM} ARE GIVEN.

Shielding [mm]	τ_{EMM}	τ_{EIM}	τ_{SVM}	τ_{DHEP}
	[Errors/day/Mbit]			
	LEO			
12.70	$1.94 \cdot 10^0$	$3.09 \cdot 10^0$	$2.88 \cdot 10^0$	$2.34 \cdot 10^0$
6.35	$6.94 \cdot 10^0$	$1.11 \cdot 10^1$	$1.03 \cdot 10^1$	$8.33 \cdot 10^0$
2.54	$5.01 \cdot 10^1$	$8.00 \cdot 10^1$	$7.45 \cdot 10^1$	$5.92 \cdot 10^1$
	GEO			
12.70	$1.49 \cdot 10^{-6}$	$2.38 \cdot 10^{-6}$	$2.22 \cdot 10^{-6}$	$1.81 \cdot 10^{-6}$
6.35	$1.20 \cdot 10^{-6}$	$1.91 \cdot 10^{-6}$	$1.78 \cdot 10^{-6}$	$1.46 \cdot 10^{-6}$
2.54	$1.04 \cdot 10^{-6}$	$1.65 \cdot 10^{-6}$	$1.54 \cdot 10^{-6}$	$1.25 \cdot 10^{-6}$
Ratio	0.67	1.07	1.00	0.79

TABLE VIII
SER FOR THE LATTICE MEMORY FOR THE LEO AND GEO RADIATION ENVIRONMENTS BEHIND VARIOUS SHIELDING THICKNESSES AFTER THE FOUR METHODS PRESENTED. ALSO THE AVERAGE RATIO OF THE DIFFERENT METHODS TO τ_{SVM} ARE GIVEN.

Shielding [mm]	τ_{EMM}	τ_{EIM}	τ_{SVM}	τ_{DHEP}
	[Errors/day/Mbit]			
	LEO			
12.70	$2.12 \cdot 10^{-3}$	$1.64 \cdot 10^{-3}$	$2.94 \cdot 10^{-3}$	$6.60 \cdot 10^{-3}$
6.35	$7.57 \cdot 10^{-3}$	$5.86 \cdot 10^{-3}$	$1.05 \cdot 10^{-2}$	$2.35 \cdot 10^{-2}$
2.54	$5.45 \cdot 10^{-2}$	$4.22 \cdot 10^{-2}$	$7.55 \cdot 10^{-2}$	$1.67 \cdot 10^{-1}$
	GEO			
12.70	$1.63 \cdot 10^{-9}$	$1.26 \cdot 10^{-9}$	$2.27 \cdot 10^{-9}$	$5.11 \cdot 10^{-9}$
6.35	$1.31 \cdot 10^{-9}$	$1.01 \cdot 10^{-9}$	$1.83 \cdot 10^{-9}$	$4.11 \cdot 10^{-9}$
2.54	$1.13 \cdot 10^{-9}$	$8.76 \cdot 10^{-10}$	$1.58 \cdot 10^{-9}$	$3.54 \cdot 10^{-9}$
Ratio	0.72	0.56	1.00	2.20

The DHEP method considers all protons below $3\,\mathrm{MeV}$ to contribute to the PDI SER. As can be seen in Fig. 2, this overestimates the width of the PDI peak and therefore the lower HEP cross-section reduces the results. For this case, this energy limit should be lowered to the actual PDI peak width, which will increase the adjusted cross-section (6) and with that the result of the SER. This holds true for devices with high PDI sensitivity like the ISSI. For the device with lower sensitivity, the DHEP SER method overestimates the SER comparatively to the QME methods. In this case, the wide energy spectrum of the degraded proton beam increases the measured cross-section stronger than for more sensitive devices, because the difference between the LEP and HEP cross-sections is much smaller in these cases. This effect outweighs the effect of the energy limit of $3\,\mathrm{MeV}$ described above for the ISSI device. Therefore, for the Lattice SRAM the DHEP method estimates the highest SER.

The agreement of the QME methods with each other depends on the closeness of the measured PDI response to the respective fitting method. As seen in Fig. 2 and Fig 3,

the fits of the experimental data by the respective QME SER method vary. Therefore, the resulting SER vary as well.

V. EXTRACTING PDI SENSITIVE VOLUME PARAMETERS FROM DEGRADED PROTON BEAM DATA

A common method to evaluate QME LEP cross-sectional data is to extract parameters for a single SV RPP geometry, also referred to as the PDI SV in this work. This geometry can be used as a surrogate in radiation transport calculations and the device can be investigated in various radiation environments without the need of further irradiation tests. A method to extract PDI SV parameters from experimental QME cross-sectional data was introduced in [36], which was benchmarked against MC simulations. In this work, the applicability of that method is shown to extend to extract PDI SV parameters from DHEP data.

A. Methods and Calculations

The method in [36] essentially uses a function of proton energy E and the SV parameters: overlayer thickness h_{OL}, SV thickness h_{SV}, side length of the front square face of the SV a_{SV}, the critical charge Q_{crit}. The method estimates the cross-sections from a given set of PDI SV parameters following these four steps:

1.) Estimation of the energy of the initial proton (of energy E) after the overlayers (h_{OL}). This is done with a numerical stopping force model.
2.) The stopping model and a numerical straggling model are used to estimate the energy deposition distribution of the proton while traversing the SV (h_{SV}).
3.) Q_{crit} is converted to MeV and applied to the energy deposition distribution. This provides the proportion of energy deposition events above Q_{crit} that upset the SV.
4.) The proportion estimated in 3.) is multiplied with the area of the SV (a_{SV}^2). This gives an estimated cross-section σ_{method}.

The estimated cross-section can be fitted to the experimental cross-section data by varying the SV parameters until the estimated and experimental cross-sections agree. This provides a way to numerically extract PDI SV parameters from QME data without the use of the MC method.

For the current application to the DHEP data, the proton SEU response σ_{method} of the device is estimated using the method presented in [36] with the following modifications for the use in context with DHEP data.

Firstly, the overlayer thickness parameter (h_{OL}) will be fixed to $0.0\,\mu m$. This parameter is very small, commonly $\ll 100\,\mu m$, compared to the thickness of the degraders (several mm) used in the DHEP method. Therefore, this parameter is not easily determined during the fitting procedure and would only increase the complexity of the computation with little to no gain.

Secondly, to accurately estimate the cross-sections resulting from the degraded spectra (Fig. 5), the high energy saturated proton cross-section is added as a fixed variable for the fitting procedure. Hence in this work, the response function

is partially defined to account for the PDI SEU peak and the saturated cross-section at high energies. Whenever the result of the method is below the value of the saturated cross-section, it is set to the value of the saturated proton cross-section. This applies only for energies above $0.06\,MeV$, at which the LET of protons is highest, therefore only after the PDI cross-section peak.

Finally, from the LET_0 value determined from the HI irradiation results, it can be assumed that the ratio of h_{SV} and Q_{crit} depends on LET_0 as follows:

$$LET_0 = \frac{Q_{crit}}{h_{SV}} \cdot C, \tag{8}$$

where C is a conversion factor of $0.0966 \, \frac{\mu m \, cm^2}{fC \, mg}$.

This alteration is made on the assumption that HI with a LET of LET_0 should be able to upset the PDI SV. Therefore, the dimensions of the resulting SV should result in the ratio of Q_{crit} and h_{SV} that is similar to LET_0.

These alterations to the method result in only two free parameters: a_{SV} and h_{SV}. These parameters are determined by fitting the estimated cross-section $\sigma_{est,d_{Al}}$ calculated from $\sigma_{method}(E, a_{SV}, h_{SV})$ to the experimental DHEP data.

The estimated cross-section $\sigma_{est,d_{Al}}$ in cm^2/bit for a given degrader configuration with Al degrader thickness d_{Al} in addition to $7\,mm$ Cu is then calculated after

$$\sigma_{est,d_{Al}} = \int_0^\infty \sigma_{method}(E, a_{SV}, h_{SV}) \cdot PDF_{d_{Al}}(E), \tag{9}$$

where $PDF_{d_{Al}}(E)$ is the probability density function of the degraded proton beam spectra for the degrader configuration with Al thickness d_{Al}.

From (9) a set of cross-sections is derived for all Al thicknesses d_{Al} for a given set of parameters for the SEU response curve σ_{alg}. The parameters of σ_{alg} are then fitted in regards to the experimental degraded proton beam data σ_{DHEP} (see Fig. 4) by comparing $\sigma_{est,d_{Al}}$ to the experimental data and minimizing Δ:

$$\Delta = \sum_{d_{Al}} [log_{10}(\sigma_{est,d_{Al}}) - log_{10}(\sigma_{DHEP,d_{Al}})]^2 \tag{10}$$

For this procedure, if more than one experimental data point exists for a given degrader configuration, the average of the available data was calculated.

The difference between the measured and simulated spectra for the low d_{Al} spectra ($0.2\,mm$ and $0.4\,mm$) seen in Fig. 5 is assumed to impact the accuracy of the fit and those spectra are therefore considered in the fitting procedure with a reduced weight of $10\,\%$. Figure 5 shows that the agreement of the simulated and measured spectra increases with higher degrader thicknesses as the the effects on the low energy tail of the spectra become less pronounced. Therefore, it is assumed that the accuracy for the extrapolated spectra, d_{Al} equal to $1.0\,mm$ and $1.5\,mm$, is just as good as for the $0.4\,mm$ and $0.6\,mm$ configurations and those are therefore included in the fitting procedure.

B. Results

The results for the fitting of the degraded beam data for ISSI and Lattice are shown in Figs. 6 and 7. The upper figure shows the experimental and calculated cross-section from the best fit of σ_{alg} DHEP cross-section data in $\mathrm{cm}^2/\mathrm{bit}$ over the Al degrader thickness d_{Al} in mm as well as from MC simulation using G4SEE toolkit [41]. In the simulation the geometry is defined using the SV parameters extracted from the fitting of the DHEP data.

The lower figure shows the experimental QME LEP and HEP SEU cross-section data as a function of proton energy at SV level in MeV. For comparison, the response functions estimated from the PDI SV parameters extracted from the QME and DHEP data are given in the lower graphs of Figs. 6 and 7.

Energy at SV level was chosen to compare the experimental data to the fitted response functions as the device overlayers were omitted from the fitting procedure. The area around the estimated response function from the fit of the DHEP data indicates the changes in the fitting results if the degrader thicknesses are to be changed by $\pm 1\%$, thereby resulting in change in the degraded spectra. One should note, the experimental QME cross-section data displayed in the lower graphs is provided here for comparison, and were not used at any point in the fitting process. The determined parameters for the PDI SV from the QME and DHEP cross-section data are given in Table IX as well as the the results of the χ^2-test of the respective fits. The PDI SV parameters extracted for the ISSI device are lower than the one extracted in [36]. The ISSI cross-section data obtained during this campaign was lower compared to the one used in [36] and therefore the extracted PDI SV parameters reflect this change in cross-section magnitude. The reason for the reduced cross-section values is considered to be caused by part and lot variations and different date codes (between the devices in this work and the work referenced in [36]) and no further investigations of potential other causes was done as this would have exceeded the scope and aim of this work.

TABLE IX
PDI SV PARAMETERS DETERMINED IN THIS WORK FOR ALL DUTs FROM THE QME AND THE DHEP SEU CROSS-SECTION DATA.

	ISSI		Lattice	
	QME	DHEP	QME	DHEP
$h_{OL,Si}$ [µm]	5.9	-	9.9	-
a_{SV} [µm]	0.08	0.06	0.0014	0.0026
h_{SV} [µm]	0.23	0.54	0.35	0.75
Q_{crit} [fC]	0.73	1.79	0.70	2.48
χ^2[cm²/bit]	$2.2 \cdot 10^{-10}$	$2.9 \cdot 10^{-4}$	$3.0 \cdot 10^{-14}$	$4.9 \cdot 10^{-4}$

C. Discussion

The extraction method for the PDI SV parameters from the DHEP SEU cross-section data provided a successful proof-of-concept. The cross-section data from highly degraded beam are linked to the device's quasi mono-energetic SEU
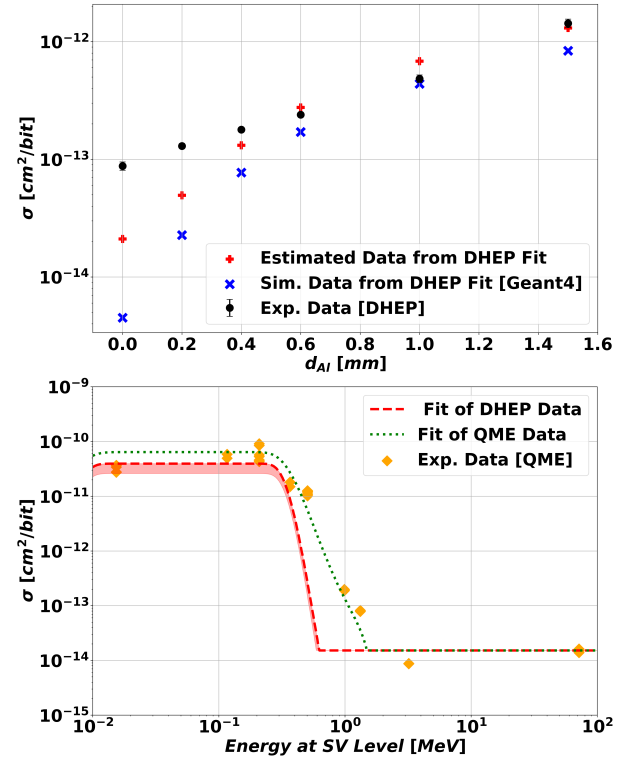

Fig. 6. *Upper:* DHEP SEU cross-sections σ in $\mathrm{cm}^2/\mathrm{bit}$ for the ISSI DUT as a function of the Al degrader thickness d_{Al}. Displayed are the experimental DHEP data (circle), estimated data from the fitted QME response (plus) as well as the results of the MC simulation based on the SV parameters obtained from the fit (cross). *Lower:* SEU cross-sections σ in $\mathrm{cm}^2/\mathrm{bit}$ obtained from QME LEP tests as a function of the proton energy at SV level in MeV, when the energy loss in the BEOL has been taken into account. The experimental QME data (diamonds) and the fitted response curves from the QME (dotted green) and the DHEP (dashed red) data are displayed. The fitted QME response from the DHEP data includes the error range caused by $\pm 1\%$ uncertainties in the thicknesses of the different degrader layers.

response. The investigation here shows that it is possible to extract single SV RPP geometry parameters from DHEP data. The PDI SV parameters can be used to simulate [41] or numerically estimate [36] the QME LEP cross-section response of the device from DHEP data. While the PDI SV parameters do not represent real physical properties of the device, they provide a useful surrogate for it in radiation transport calculations.

For the ISSI device, the fitting procedure resulted in a set of parameters that produces a similar SEU response as the experimental QME cross-section data. The response functions estimate the DHEP data well with the simulated degraded proton spectra. For the Lattice device the extracted PDI SV parameters and the associated SEU response curve differ more from the experimental data. The PDI SV parameters (see Table IX) extracted from the QME and DHEP cross-section data differ slightly for the ISSI and slightly more for the Lattice. Overall, the method in this work extracted PDI SV parameters with shorter h_{SV} and higher Q_{crit} compared to the parameters extracted directly from the QME data. This causes the resulting response to be narrower than for the
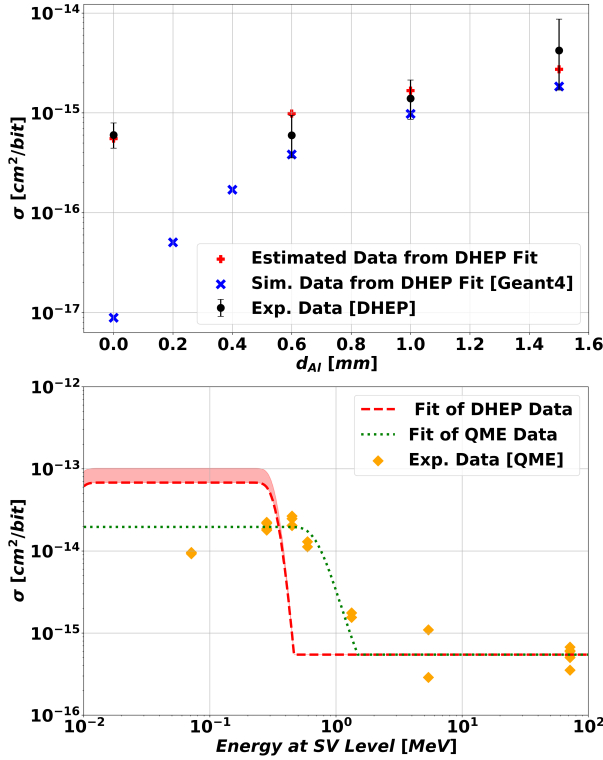
Fig. 7. *Upper:* DHEP SEU cross-sections σ in $\mathrm{cm}^2/\mathrm{bit}$ for the Lattice DUT as a function of the Al degrader thickness d_{Al}. Displayed are the experimental DHEP data (circle), estimated data from the fitted QME response (plus) as well as the results of the MC simulation based on the SV parameters obtained from the fit (cross). *Lower:* SEU cross-sections σ in $\mathrm{cm}^2/\mathrm{bit}$ from QME LEP tests as a function of the proton energy at SV level in MeV with the energy loss in the BEOL taken into account. The experimental QME data (diamonds) and the fitted response curves from the QME (dotted green) and the DHEP (dashed red) data are displayed. The fitted QME response from the DHEP data includes the error range caused by $\pm 1\%$ uncertainties in the thicknesses of different degrader layers.

parameters extracted from the QME data. The values for a_{SV} from the QME and DHEP data differ by a factor of 0.75 for ISSI and a factor of 1.85 for Lattice. The face area of the SV, a_{SV}^2, equals the maximum cross-section of the device. Therefore, the PDI SV parameters provide direct insight about the height of the PDI peak. Further, the shape of the PDI peak can be estimated from the PDI SV parameters [36] as seen in Figs. 6 and 7. Overall, the estimated QME PDI cross-section response from the PDI SV parameters extracted from the DHEP data exhibit good agreement with the measured QME data for ISSI and less similarity for the Lattice device. Furthermore, the PDI SV parameters reproduced the experimental DHEP data well in Geant4 simulations for the higher degrader thicknesses.

The biggest difference between the experimental and the estimated DHEP data can be seen for $0.0\,\mathrm{mm}$ and $0.2\,\mathrm{mm}$ d_{Al}. This is due to the fact that those were not considered fully in the fitting procedure and the limited agreement of the measured spectra versus the simulated spectra for low degrader thicknesses, which might be caused by scaling effects from the collimator that could not be taken into account in the simulated spectra. This difference is even

more pronounced in the MC simulation as the simulation only considered a single volume for the PDI SV, hence the cross-section is reduced for the degrader thicknesses that are associated with a higher proportion of high energy protons in the spectra, which would require nested SVs to be accurately considered in MC simulations.

One limitation of the method seems to be the amount of data points taken during the DHEP measurements. This is indicated by the fact that the method was able to reproduce the measured QME response better for the ISSI device which had six data points than for the Lattice with only four data points. This a common behavior for fitting processes. But this effect could also be caused by the difference in PDI sensitivity of the two devices. Furthermore, this method should be reliant on the accuracy of the measured or simulated beam spectra, and it is a great challenge to measure spectra ranging over a wide energy range properly, especially down to low energies around hundreds of keV. Since the low energy part of the spectra is of great importance as it contributes to the PDI peak the most, the quality of the measured or simulated spectra might impact the determined PDI SV parameters.

To reduce the potential effects of these factors, the inclusion of the LET_0 value from the Weibull fit obtained for HI data was implemented. It reduces the amount of variable parameters in the proton model to be fitted and therefore allowed for more accurate results.

Despite the limited amount of data acquired in this work, and the reliance on MC simulation to supplement the measured spectra, the proposed method provided acceptable results that demonstrates a proof-of-concept, that has the potential to provide more accurate PDI SV parameters from data obtained with degraded high energy proton beams, when more data points and more accurate spectra are available than in this work.

VI. DISCUSSION ON TEST METHODS

A. Preparation & Tests

In order to perform quasi mono-energetic LEP measurement, access to a suitable LEP facility is necessary. The facility needs to provide sufficiently low primary proton energies, with good energy resolution, and reliable energy selection. The main preparation to be performed for the QME method is the delidding of the devices to limit the amount of overlayer material between the SV of the DUT and the incoming beam to reduce energy straggling.

For the DHEP approach, a facility with an appropriately high initial proton beam energy (i.e., tens of MeV) is required, so that the degraded beam spectrum fulfills the requirements for the method. In order to check whether the requirement is fulfilled, preliminary radiation transport calculations (e.g., Geant4, SRIM [43], ...) have to be performed with the degrader material(s) chosen for the campaign. Additionally, means to insert additional degrader material into the beam line at the facility might have to be found as the present degrader materials might not be enough or do not allow for sufficient resolution. Before performing the actual measurements, the resulting spectra and fluxes of the

degraded proton beam have to be determined accurately at the DUT level for all the degrader configurations used. This is required to determine the flux at DUT level accurately as well as compare the degraded spectra with the simulation results to benchmark the simulation setup. If the energy spectra are measured with high resolution ranging from low (several keV) to high (several MeV) proton energies, simulations might not be necessary. However, for cross-checking purposes, simulations are highly recommended regardless of the quality of the experimental spectra.

The irradiations for the QME method are performed in vacuum due to the low range of the LEPs in air, while the DHEP method can be performed in air, because the air can be considered as part of the degrader set up. This makes access to the DUT during the campaign quicker and easier and allows for more flexibility in the test planning.

B. Results & Post-Processing

For the QME method, the minimum requirement is to know the fluence and the beam energy. This information is typically provided by the facility. With this, the cross-section as a function of proton energy can be calculated. Uncertainties could arise from the flux monitoring as well as the width of the proton beam spectra, which is commonly narrow enough to be negligible. The method will directly provide reliable information on the devices response to protons at a given energy. This information can be used directly in a variety of SER calculations as well in the construction of a PDI SV RPP geometry for the DUT without any further data.

For the DHEP approach only one SER approach has been formulated, thereby limiting the choice of SER estimation methods. The SER method requires at least knowledge about the degraded beam spectra for the degrader configuration for which the peak cross-section is observed. High energy proton facilities do not perform these kinds of measurements commonly and require additional measurements to the present beam monitoring. Investments into acquisition and set up of new detectors for accurate spectrum measurements have to be done by either the facility or the user. Furthermore, due to the nature of this approach the SEU cross-section data obtained by this method do not easily allow for further insights from the data outside of the SER calculation.

The proof-of-concept presented in this work shows that it is possible to determine PDI SV parameters from DHEP data, but it requires a high accuracy in the measured or simulated spectra as well as a high number of cross-section values. This makes the estimation of PDI SV parameters with this method more difficult and time consuming compared to the QME approach.

VII. CONCLUSIONS & FUTURE WORK

In conclusion, the QME method is the preferable way of testing for PDI SEU cross-sections. Its advantages are in the ease of the irradiation procedure, the post processing and the usability of the data. The DHEP data requires detailed knowledge over the energy spectra of the degraded beam for any further use of the cross-section data. This demands accurate dosimetry and simulations, which are difficult and time consuming, and most facilities are not adequately equipped for this novel approach. Nevertheless, both methods provide similar SERs and indication of PDI sensitivity. This means that both methods are viable ways to perform these investigations, while the DHEP method is more prone to uncertainties. Furthermore, the DHEP method provides its own unique advantages. It allows LEP measurements to be performed with a high energy proton beam if no low energy beam is available or accessible. Also, it does not necessarily require any delidding of the components, as the packaging can be considered as part of the degrader configurations, making this method a good alternative when device preparation cannot be performed. Because the irradiations are performed in air, adjusting the DUT and investigating several roll and tilt configurations is much easier than for the QME measurements performed in vacuum.

Overall, it is an advantage to have alternative measurement methods, even though the DHEP method does not replace the QME method. This is partly due to fact, that the QME method is more established. The DHEP method predominantly suffers from the uncertainties in flux and spectrum measurements and potential simulations. If HEP facilities were inherently prepared to offer DHEP services, the severeness of those uncertainties would decrease. Potentially, simulations may not be necessary anymore, when spectrum measurements increase in accuracy.

Finally, this work presented a proof-of-concept approach to extract the PDI SEU response function and the associated SV parameters from the DHEP data. Thereby proposing that the results of the two test methods can be interchangeable as the QME cross-section response can be simulated or numerically estimated from the PDI SV parameters. This approach requires detailed knowledge about the degraded beams, even more than for the DHEP SER method, and a high amount of data points to accurately estimate the response function accurately, making the approach more complex and time intensive. It is not a replacement for the direct QME method to obtain the QME cross-section curve, but it bridges the gap from DHEP data to QME data, both in concept and in application.

The method presented here and its underlying method have been shown to extract PDI SV parameters for devices with technology nodes of $40\,\mathrm{nm}$ and above. The validity of this numerical approach for smaller technology sizes has to be investigated further. With smaller technology sizes, unaccounted effects on the LEP cross-section can emerge that are not considered in the current iteration of the method. Nevertheless, the method does require little to no prior knowledge of the device parameter to determine a set of PDI SV parameters. Only the overlayer thickness cannot be estimated from DHEP data alone.

Further work is required to assess the optimal accuracy of the spectra and the amount of data points used as well as on the uniqueness of the fit results and its dependency on

the initial parameters, however the latter two also depend strongly on the fitting procedure chosen. The amount of data taken for this work is too limited to perform such investigations. When this method is further investigated it has the potential to enhance the DHEP method to extract PDI SV parameters and from that estimate the QME SEU cross-section data using degraded high energy beams.

The method presently benefits greatly from the HI data, specifically LET_0, to provide more accurate results for the presented amount of DHEP data points. This makes the extraction of PDI SV parameters from DHEP data dependent on HI data, unlike the extraction from QME data. This is not a great drawback, because HI irradiations are commonly performed on most devices. Further research is required to determine whether a higher amount of data points and more accurate beam spectra would allow this method to perform as well without the use of the HI data.

More detailed investigation of the general connection of PDI LEP and HI data are of interest but are beyond the scope of this paper.

ACKNOWLEDGMENTS

REFERENCES

[1] ECSS, "Single event effects test method and guidelines - ESCC basic specification no. 25100," tech. rep., ESA, Oct. 2014.

[2] J. R. Schwank, M. R. Shaneyfelt, and P. E. Dodd, "Radiation hardness assurance testing of microelectronic devices and integrated circuits: Test guideline for proton and heavy ion single-event effects," *IEEE Trans. Nucl. Sci.*, vol. 60, no. 3, pp. 2101–2118, Jun. 2013.

[3] H. Zhang *et al.*, "Angular effects of heavy-ion strikes on single-event upset response of flip-flop designs in 16-nm bulk FinFET technology," *IEEE Trans. Nucl. Sci.*, vol. 64, no. 1, pp. 491–496, Jan. 2017.

[4] H. Nakajima *et al.*, "Single event effect characterization of the mixed-signal ASIC developed for CCD camera in space use," *Nucl. Instrum. Methods Phys. Res., Sect. A*, vol. 731, pp. 166–171, Dec. 2013.

[5] D. Chen *et al.*, "Heavy ion and proton-induced single event upset characteristics of a 3-D NAND flash memory," *IEEE Trans. Nucl. Sci.*, vol. 65, no. 1, pp. 19–26, Jan. 2018.

[6] D. Chen *et al.*, "Heavy ion irradiation fluence dependence for single-event upsets in a NAND flash memory," *IEEE Trans. Nucl. Sci.*, vol. 64, no. 1, pp. 332–337, Jan. 2017.

[7] R. K. Lawrence and A. T. Kelly, "Single event effect induced multiple-cell upsets in a commercial 90 nm CMOS digital technology," *IEEE Trans. Nucl. Sci.*, vol. 55, no. 6, pp. 3367–3374, Dec. 2008.

[8] E. P. Wilcox *et al.*, "Observation of low-energy proton direct ionization in a 72-layer 3-D NAND flash memory," *IEEE Trans. Nucl. Sci.*, vol. 68, no. 5, pp. 835–841, May 2021.

[9] A. Coronetti *et al.*, "Assessment of proton direct ionization for the radiation hardness assurance of deep submicron SRAMs used in space applications," *IEEE Trans. Nucl. Sci.*, vol. 68, no. 5, pp. 937–948, May 2021.

[10] J. Wang, J. Prinzie, A. Coronetti, S. Thys, R. G. Alia, and P. Leroux, "Study of SEU sensitivity of SRAM-based radiation monitors in 65-nm CMOS," *IEEE Trans. Nucl. Sci.*, vol. 68, no. 5, pp. 913–920, May 2021.

[11] C. Peng *et al.*, "Low-energy proton-induced single event effect in NAND flash memories," *Nucl. Instrum. Methods Phys. Res., Sect. A*, vol. 969, pp. 1–7, Jul. 2020. Art. no. 164064.

[12] K. P. Rodbell, "Low-energy protons - where and why 'rare events' matter," *IEEE Trans. Nucl. Sci.*, vol. 67, no. 7, pp. 1204–1215, Jul. 2020.

[13] Z. Wang *et al.*, "Proton-induced single-event effects on 28 nm Kintex-7 FPGA," *Microelectron. Reliab.*, vol. 107, pp. 1–6, Apr. 2020. Art. no. 113594.

[14] R. G. Alia *et al.*, "Direct ionization impact on accelerator mixed-field soft-error rate," *IEEE Trans. Nucl. Sci.*, vol. 67, no. 1, pp. 345–352, Jan. 2019.

[15] Y. Luo, F. Zhang, X. Pan, H. Guo, and Y. Wang, "Impact of total ionizing dose on low energy proton single event upsets in nanometer SRAM," *IEEE Trans. Nucl. Sci.*, vol. 66, no. 7, pp. 1848–1853, Jul. 2019.

[16] J. Guillermin, N. Sukhaseum, P. Pourrouquet, N. Chatry, F. Bezerra, and R. Ecoffet, "Worst-case proton contribution to the direct ionization SEU rate," *Eur. Conf. Radiat. Its Eff. Compon. Syst., 17th, Geneva, Switzerland*, pp. 330–337, Oct. 2017.

[17] K. P. Rodbell, M. S. Gordon, K. G. Stawiasz, P. Oldiges, K. Lilja, and M. Turowski, "Low energy proton SEUs in 32-nm SOI SRAMs at low Vdd," *IEEE Trans. Nucl. Sci.*, vol. 64, no. 3, pp. 999–1005, Mar. 2017.

[18] V. Gupta *et al.*, "SEE on different layers of stacked-SRAMs," *IEEE Trans. Nucl. Sci.*, vol. 62, no. 6, pp. 2673–2678, Dec. 2015.

[19] J. A. Pellish *et al.*, "Criticality of low-energy protons in single-event effects testing of highly-scaled technologies," *IEEE Trans. Nucl. Sci.*, vol. 61, no. 6, pp. 2896–2903, Dec. 2014.

[20] J. Wert *et al.*, "Low-energy proton testing using the Boeing Radiation Effects Laboratory 2.2 MeV dynamitron," *2012 IEEE Radiat. Eff. Data Workshop, Miami, FL, USA*, pp. 64–69, Jul. 2012.

[21] H. Puchner, J. Tausch, and R. Koga, "Proton-induced single event upsets in 90nm technology high performance SRAM memories," *2011 IEEE Radiat. Eff. Data Workshop, Las Vegas, NV, USA*, pp. 161–163, Jul. 2011.

[22] N. Seifert, B. Gill, J. A. Pellish, P. W. Marshall, and K. A. Label, "The susceptibility of 45 and 32 nm bulk CMOS latches to low-energy protons," *IEEE Trans. Nucl. Sci.*, vol. 58, no. 6, pp. 2711–2718, Dec. 2011.

[23] B. D. Sierawski *et al.*, "Impact of low-energy proton induced upsets on test methods and rate predictions," *IEEE Trans. Nucl. Sci.*, vol. 56, no. 6, pp. 3085–3092, Dec. 2009.

[24] D. F. Heidel *et al.*, "Single-event upsets and multiple-bit upsets on a 45 nm SOI SRAM," *IEEE Trans. Nucl. Sci.*, vol. 56, no. 6, pp. 3499–3504, Dec. 2009.

[25] D. F. Heidel *et al.*, "Low energy proton single-event-upset test results on 65 nm SOI SRAM," *IEEE Trans. Nucl. Sci.*, vol. 55, no. 6, pp. 3394–3400, Dec. 2008.

[26] K. P. Rodbell, D. F. Heidel, H. H. K. Tang, M. S. Gordon, P. Oldiges, and C. E. Murray, "Low-energy proton-induced single-event-upsets in 65 nm node, silicon-on-insulator, latches and memory cells," *IEEE Trans. Nucl. Sci.*, vol. 54, no. 6, pp. 2474–2479, Dec. 2007.

[27] N. A. Dodds *et al.*, "The contribution of low-energy protons to the total on-orbit SEU rate," *IEEE Trans. Nucl. Sci.*, vol. 62, no. 6, pp. 2440–2451, Dec. 2015.

[28] N. A. Dodds *et al.*, "Hardness assurance for proton direct ionization-induced SEEs using a high-energy proton beam," *IEEE Trans. Nucl. Sci.*, vol. 61, no. 6, pp. 2904–2914, Dec. 2014.

[29] E. H. Cannon *et al.*, "Heavy ion, high-energy, and low-energy proton SEE sensitivity of 90-nm RHBD SRAMs," *IEEE Trans. Nucl. Sci.*, vol. 57, no. 6, pp. 3493–3499, Dec. 2010.

[30] M. Glorieux and T. Bonnoit, "Radiation results of SER tests standard test report - R1RW0416DSB - V 1.0," tech. rep., IROC Technologies, Dec. 2018.

[31] M. Glorieux, "Radiation results of SER tests standard test report - Xilinx XZU3EG - V 1.4," tech. rep., IROC Technologies, Dec. 2018.

[32] R. K. Lawrence, J. F. Ross, N. F. Haddad, R. A. Reed, and D. R. Albrecht, "Soft error sensitivities in 90 nm bulk CMOS SRAMs," *2009 IEEE Radiat. Eff. Data Workshop, Quebec, QC, Canada*, pp. 123–126, Jul. 2009.

[33] N. F. Haddad *et al.*, "Incremental enhancement of SEU hardened 90 nm CMOS memory cell," *IEEE Trans. Nucl. Sci.*, vol. 58, no. 3, pp. 975–980, Jun. 2011.

[34] G. Augustin, N. Sukhaseum, A. Varotsou, and J. Guillermin, "Risk assessment of SEE events due to high energy electrons during the JUICE mission- final report," tech. rep., TRAD Tests & radiations, Feb. 2018.

[35] J. R. Schwank *et al.*, "Hardness assurance testing for proton direct ionization effects," *IEEE Trans. Nucl. Sci.*, vol. 59, no. 4, pp. 1197–1202, Aug. 2012.

[36] S. Lüdeke and A. Javanainen, "Proton direct ionization in sub-micron technologies: Numerical method for RPP parameter extraction," *IEEE Trans. Nucl. Sci.*, vol. 69, no. 3, pp. 254–263, Mar. 2022.

[37] "RADiation Effects Facility - department of physics." https://www.jyu.fi/science/en/physics/research/infrastructures/accelerator-laboratory/radiation-effects-facility. Accessed: 14.06.2022.

[38] "Heavy ion facility at UC Louvain." https://uclouvain.be/en/research-institutes/irmp/crc/heavy-ion-facility-hif.html. Accessed: 11.08.2022.

[39] H. Kettunen *et al.*, "Low energy protons at RADEF-application to advanced eSRAMs," *IEEE Radiat. Eff. Data Workshop, Paris, France*, pp. 304–307, Jul. 2014.

[40] W. Hajdas, L. Adams, B. Nickson, and A. Zehnder, "The Proton Irradiation Facility at the Paul Scherrer Institute," *Nucl. Instrum. Methods Phys. Res., Sect. B*, vol. 113, no. 1-4, pp. 54–58, Jun. 1996.

[41] D. Lucsanyi, R. G. Alia, K. Bilko, M. Cecchetto, S. Fiore, and E. Pirovano, "G4SEE: A Geant4-based single event effect simulation toolkit and its validation through monoenergetic neutron measurements," *IEEE Trans. Nucl. Sci.*, vol. 69, no. 3, pp. 273–281, Feb. 2022.

[42] S. Agostinelli *et al.*, "GEANT4 - a simulation toolkit," *Nucl. Instrum. Methods Phys. Res., Sect. A*, vol. 506, no. 3, pp. 250–303, Jul. 2003.

[43] J. F. Ziegler, "SRIM-2003," *Nucl. Instrum. Methods Phys. Res., Sect. B*, vol. 219-220, no. 1-4, pp. 1027–1036, Jun. 2004.